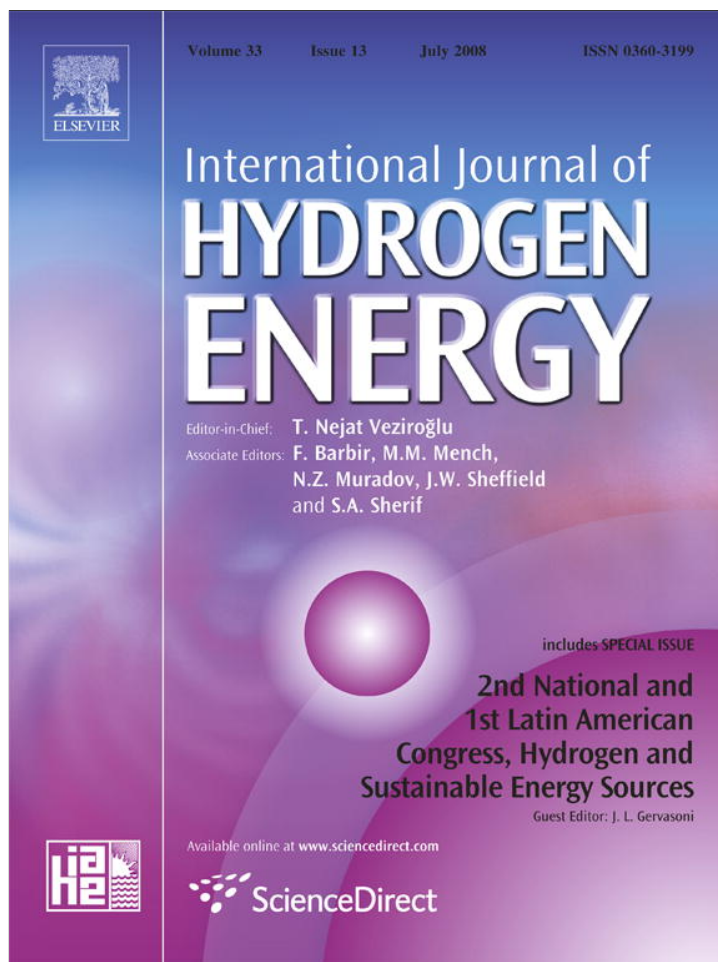


Provided for non-commercial research and education use.
Not for reproduction, distribution or commercial use.



This article appeared in a journal published by Elsevier. The attached copy is furnished to the author for internal non-commercial research and education use, including for instruction at the authors institution and sharing with colleagues.

Other uses, including reproduction and distribution, or selling or licensing copies, or posting to personal, institutional or third party websites are prohibited.

In most cases authors are permitted to post their version of the article (e.g. in Word or Tex form) to their personal website or institutional repository. Authors requiring further information regarding Elsevier's archiving and manuscript policies are encouraged to visit:

<http://www.elsevier.com/copyright>

Available at www.sciencedirect.comjournal homepage: www.elsevier.com/locate/ijhe

Neutron imaging investigation of liquid water distribution in and the performance of a PEM fuel cell [☆]

J. Park^a, Xianguo Li^{a,*}, D. Tran^b, T. Abdel-Baset^b, D.S. Hussey^c, D.L. Jacobson^c, M. Arif^c

^aDepartment of Mechanical Engineering, University of Waterloo, 200 University Ave W., Waterloo, Ontario, Canada N2L 3G1

^bDaimlerChrysler Corporation, Auburn Hills, MI 48326, USA

^cNational Institute of Standards and Technology, Gaithersburg, MD 20899-8461, USA

ARTICLE INFO

Article history:

Received 28 October 2006

Received in revised form

15 March 2008

Accepted 16 March 2008

Available online 16 June 2008

Keywords:

Neutron radiography

Neutron imaging

PEM fuel cell

Liquid water distribution

Liquid water measurement

Performance hysteresis

ABSTRACT

In this study neutron radiography is applied to investigate the performance of a polymer electrolyte membrane (PEM) fuel cell based on the effect of liquid water accumulation in the cell. Dynamic performance tests have been carried out on a PEM fuel cell with a specially designed serpentine flow channel under various operating conditions and simultaneous measurements of accumulated liquid water with neutron imaging. Liquid water tends to accumulate in the gas diffusion layer (GDL) adjacent to the flow channel area while the liquid water formed in the GDL next to the channel land area seems to be effectively removed by the cross leakage flow through the porous GDL between the adjacent flow channels. The amount of liquid water accumulation in the cell is dependant on the cell operating temperature, the pressure drop in the flow channel and the current density under the present test conditions of fixed stoichiometry. It is shown that the cell performance is strongly affected by the presence and accumulation of liquid water, especially at high current densities. This phenomenon results in performance hysteresis for load variations. The rate of liquid water production is also mathematically modeled to analyze the effect of the cell operating temperature and pressure drop on the liquid water formation in a cell. The model result shows good agreement with experimental measurements. The history of liquid water accumulation is also analyzed.

© 2008 International Association for Hydrogen Energy. Published by Elsevier Ltd. All rights reserved.

1. Introduction

Water management is one of the critical issues for the design and operation of polymer electrolyte membrane (PEM) fuel cells since the accumulation and transport of liquid water in the PEM fuel cell can significantly deteriorate the PEM fuel cell performance [1,2]. Water is usually provided to the PEM fuel cell through the fully humidified anode and cathode gas

stream in order to provide adequate hydration for the polymer membrane electrolyte. On the other hand, water is produced at the cathode of the cell as a part of electrochemical reaction. Water is also transported inside the cell through a number of mechanisms [1]: the electroosmotic drag effect transports water from the anode to the cathode side, back diffusion occurs due to the concentration difference between the cathode and the anode side and water convec-

[☆] Certain trade names and company products are mentioned in the text or identified in an illustration in order to adequately specify the experimental procedure and equipment used. In no case does such identification imply recommendation or endorsement by the National Institute of Standards and Technology, nor does it imply that the products are necessarily the best available for the purpose.

*Corresponding author.

E-mail address: x6li@uwaterloo.ca (X. Li).

Nomenclature			
A_{cell}	active cell area, m^2	V	average velocity, m s^{-1}
C_f	wall friction coefficient	Y	mole fraction
C_l	laminar wall friction coefficient	Greek letters	
$C_{\text{cr,l}}$	correction number for pressure correlation (laminar flow)	Δ	difference
$C_{\text{cr,t}}$	correction number for pressure correlation (turbulent flow)	ζ	stoichiometry
d_h	flow channel hydraulic diameter, mm	μ	viscosity, N s m^{-2}
F	faraday constant, $96485 \text{ C mole}^{-1}$	ρ	density, kg m^{-3}
H	rate of heat transfer, kW	σ	neutron cross section
I	intensity of transmitted neutron beam	Subscripts	
I_0	intensity of incident neutron beam	0	initial/inlet value
J	cell current density, A m^{-2}	A	anode
L	flow channel length, m	A_In	anode inlet
\dot{m}	mass flow rate, kg s^{-1}	C	cathode
N	atom density	C_In	cathode inlet
N_{cell}	number of cell	ch	flow channel
\dot{N}	molar flow rate, mol s^{-1}	c, cell	fuel cell
\dot{N}_R	rate of reactant consumption in the catalyst layer, mol s^{-1}	f	friction
P	pressure, Pa	H_2	hydrogen
P_{sat}	saturation pressure of liquid water, Pa	H_2O	water
Q	volume flow rate, m^3/s	O_2	oxygen
R	universal gas constant, $8.314 \text{ kJ kmol}^{-1} \text{ K}^{-1}$	In	in/inlet value
Re	Reynolds number	k	species number
RH	relative humidity	l	laminar flow
t	equivalent thickness of liquid water layer	out	out/Outlet value
T	temperature, K	R	reacting
		t	turbulent flow

tion may be present as a result of the pressure gradient. Further, liquid water can also form due to the relative increase of the water vapor concentration in the gas stream arising from the depletion of the reactant gas species, especially at the anode if pure hydrogen is provided as the fuel. The presence of liquid water in the cell structure can have an adverse impact on the cell performance. The performance loss resulting from liquid water accumulation in the cell components is often referred to as water flooding. Measuring the amount and accumulation of the liquid water in an operating PEM fuel cell is crucial to understand the nature of flooding and or membrane drying although it is highly difficult to do so. As a result, significant thrust has been built in investigating liquid water formation and distribution in PEM fuel cells.

One of the simplest methods to measure the amount of liquid water formation in the cell is to weigh the cell before and after the cell operation [3], in addition to other ex situ measurements. Empirical techniques have also been used to analyze and diagnose the water distribution in PEM fuel cells [4,5], e.g., Mench et al. [4] used gas chromatography to provide in situ measurement of the water vapor distribution in the gas flow channels. On the other hand, liquid water formation and movement in the flow channel have been recently visualized with the use of optically accessible flow channels and digital photography [2,6–9]. These conventional optical imaging

methods through the transparent window, however, suffer a number of disadvantages, including the change of the channel surface conditions (optically accessible window surface is not the same as the typical flow channel surface built on the bipolar plates), and more importantly, the fogging of the windows due to the higher temperature and almost fully saturated gas stream in the flow channels (as compared to the ambient temperature). These issues not only complicate and obscure measurements and observations, but also question the relevance of the measurements to the real fuel cell operation. As a result, more advanced imaging techniques have recently been used to provide in situ measurement of liquid water formation and distribution in PEM fuel cells, including scanning electron microscopy [10,11], nuclear magnetic resonance microscopy [12,13], and neutron radiography [14–21].

Neutron radiography is a relatively new and attractive technique to quantify the amount and distribution of liquid water in PEM fuel cells, due to the neutron's sensitivity to hydrogen atoms in water. Since most of the PEM fuel cell components are transparent to the neutron beam, this technique enables quantification of liquid water accumulated in the entire PEM fuel cell structures including gas diffusion layers (GDLs) and gas flow channels. This technique provides an in situ, non-destructive diagnosis of liquid water formation and distribution for a live PEM fuel cell in normal

operation without restrictions. The technique has been successfully applied to PEM fuel cells and improved over the years by a few research groups to quantify the liquid water content in a PEM fuel [14–21]. Pekula et al. [19] conducted visualization study of two-phase flow in an operating PEM fuel cell by neutron imaging technique, and they found that liquid water tended to accumulate along or under the channel walls (or lands), especially at high current densities. Chuang et al. [22] found that small amount of liquid water can cause significant voltage loss at high current densities. In their work, masking techniques were utilized to distinguish the liquid water present in the flow channels and land area. Neutron imaging was extended to a tomography technique by taking pictures from different angles and a digital 3-dimensional reconstruction was made for a dry cell [16]. Hickner et al. [23] showed that the water content in a PEM fuel cell is not simply proportional to current density, but can decrease with increasing current density. In Zhang et al. [21] the influence of material on liquid water formation was visualized and the results were related to the relevant operating conditions. However, in all these previous studies, the flow channels used are simple serpentine type of short length with only a few turns of the channels. As a result, the observed characteristics of liquid water formation, distribution and dynamics may not be representatives of what happens in practical PEM fuel cells. This is because liquid water in the cell structure is known to be predominantly influenced by the flow channel designs, and the flow channels in practical PEM fuel cells are typically much longer, resulting in significant cross leakage flow through the porous GDL between the adjacent flow channels or the successive turns of the flow channel [24,25]. This cross leakage flow helps to remove the liquid water in the GDL adjacent to the flow channel.

In the present study, the accumulation of liquid water was quantified using neutron radiography for a live PEM fuel cell with a thin and long serpentine flow channel typically found

in practical PEM fuel cells. The flow channel is specially designed to effectively remove water formed in the cell by the reactant gas stream [26]. The characteristics of liquid water distribution under two different types of dynamic loading have been investigated based on the neutron images acquired and quantitative data of liquid accumulation obtained from post-processing. The amount of liquid water formed is also mathematically modeled to account for the effect of temperature on the accumulation of liquid water in a wide range of current densities. The model results are compared to the experimental measurements to provide an analysis on the steady-state amount of liquid water within the cell structure under various load conditions.

2. Experimental

Fig. 1 shows a schematic diagram of a PEM fuel cell for the present neutron imaging experiment. A PEM fuel cell consists of a membrane electrolyte assembly (MEA) sandwiched between two bipolar plates. The GDL (electrode backings), catalyst layer and PEM are referred to as an MEA where current is produced. Fuel and oxidant are supplied to either side of the MEA through flow channels on the bipolar plates producing electrons and protons in the anode catalyst layer and water in the cathode catalyst layer. Single cell test fixtures with active areas of 100.1 cm^2 were assembled using Nafion[®] 112 membrane. All parameters of cell elements are given in Table 1.

The neutron radiography system at the National Institute of Standard and Technology (NIST, Gaithersburg, USA) was used for the present study. Fig. 1 illustrates neutron radiography to image the liquid water produced in a PEM fuel cell. The neutron beam attenuates hydrogenous material, such as liquid water, while it passes through an operating PEM fuel cell. A flat panel amorphous silicon detector with $127\text{ }\mu\text{m}$ pixel pitch was used to capture the neutron image of liquid water

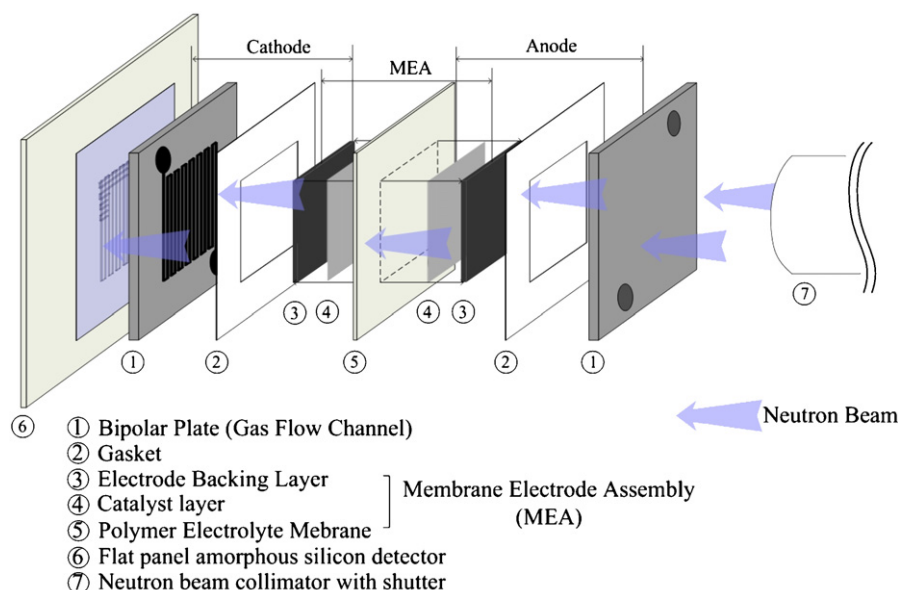


Fig. 1 – Schematic of a PEM fuel cell and neutron radiography setup.

Table 1 – Parameters for the test cell

Parameter	Value
Bipolar plate	
Number of channel (N_{ch})	1
Number of U-turn (N_{turn})	50
Channel width (w)	1.0 mm
Land width (s)	1.0 mm
Channel depth (d)	1.1 mm
Channel length (l)	5.05 m
Channel hydraulic diameter (d_h)	1.0476 mm
Cell active area (A_c)	100.1 cm ²
Membrane (Nafion[®] 112)	
Catalyst loading	0.5 mg PT cm ⁻²
Thickness (δ_n)	50 μm
Gas diffusion layer (SL Carbon Sigracet 10BB .0165")	
Permeability (K)	10 ⁻¹¹ m ²
Porosity (ϵ)	0.5
Thickness (δ_e)	200 μm
Pressure drop [25]	
Cathode (at 0.5 A/cm ² , 100% RH)	72 kPa
Anode (at 0.5 A/cm ² , 100% RH)	8 kPa

Table 2 – Experimental conditions for the dynamic tests

Parameter	Value
Constants	
Stoichiometry	1.2 (anode), 2.0 (cathode)
Inlet relative humidity (%)	100 (anode, cathode)
Outlet pressure (atm)	1
Variables	
Temperature (°C)	60, 80
Current density (A/cm ²):	
Case I	0 → 0.05 → 0.25 → 0.5 → 0.75 → 0.5 → 0.25 → 0.05 → 0
Case II	0 → 0.05 → 0.25 → 0.5 → 0.75 → 1.0 → 0.75 → 0.5 → 0.25 → 0.05 → 0
Time duration	3, 5 min for each load

in the fuel cell. The resultant is the shadow image of neutron beam attenuation with the intensity given by

$$I = I_0 e^{-N\sigma t}, \quad (1)$$

where I is the transmitted intensity, I_0 is the incident intensity (with no attenuation), N is the atom density, σ is the neutron cross-section and t is the equivalent thickness of a liquid water layer [16]. The real density of the material, Nt , is determined from I , I_0 and σ which are measured in this experiment. The raw image was analyzed using the IDL programming language (RSI, Inc., Boulder, CO) with specialized analysis routines developed at NIST. The images were taken continuously at the rate of 1 Hz during normal fuel cell operation. The fuel cell was operated according to two different unsteady load conditions; the current density was changed between 0 and 0.75 A/cm² in Case I and between 0 and 1.0 A/cm² in Case II. Details of test conditions are given in Table 2. A reference image (dry image) was taken after the MEA had been dried in the cell for at least 15 min with dry flowing nitrogen gas. The cell features that do not change with water content (such as cell hardware, background features) are subtracted by the dry image and not visible in the resulting image. The flow channel layouts are schematically given in Fig. 2 to explain how the anode and cathode flow channels overlap in the neutron images which are the resultant integration of attenuation along the beam path. A few masks are applied to distinguish the water location in the neutron images as indicated in the area diagram of Fig. 2. The average water thickness is then obtained from the natural log of the ratio of the wet to dry intensities [23]. A more detailed description of the present neutron imaging technique can be found elsewhere [15,16,23].

2.1. Mathematical modeling of liquid water production

There are a number of previous multi-dimensional numerical simulations on PEM fuel cells including liquid water transport in serpentine channels [32] and two-phase flow and chemical reactions [33,34]. However numerical simulation of dynamic liquid water distribution in PEM fuel cells is still a challenging task demanding large computing power, especially with strong cross flow through the GDL between the adjacent flow channels. In this section, a mathematical model is formulated to predict the amount of liquid water formation in an operating PEM fuel cell. The rate of liquid water production is dependant on the inlet humidity, cell temperature, pressure drop and current density (the rate of reaction) for a fixed stoichiometry operation. The rate of liquid water production may not be calculated directly from the inlet conditions since all these parameters are strongly coupled. Fig. 3 shows a schematic flow diagram of heat and mass transfer for present modeling. The serpentine flow channel on the bipolar plate is modeled as up and downstream segments with one reaction site where the electro-chemical reaction and heat transfer occur. Pressure drop is calculated based on the assumption that there is no reaction for the upstream part while the reaction is completed for the downstream part. The pressure, temperature and compositions are assumed to be uniform in each of loop segment. The inlet hydrogen and oxygen molar flow rates to the anode and cathode are determined according to the stoichiometry:

$$\dot{N}_{H_2} = \frac{\zeta_A N_{cell} J A_{cell}}{2F}, \quad (2)$$

$$\dot{N}_{O_2} = \frac{\zeta_C N_{cell} J A_{cell}}{4F}, \quad (3)$$

where ζ_A and ζ_C are the anode and cathode stoichiometries, N_{cell} is the number of cells in the stack, which is taken as one in the present study, J is the current density, A_{cell} is the active area of the cell, and F is the Faraday constant. The inlets of the anode and cathode flow channels are saturated with water vapor. The total flow rates are obtained by adding the amount of water vapor to that of hydrogen for the anode stream and by adding the amount of water and nitrogen to

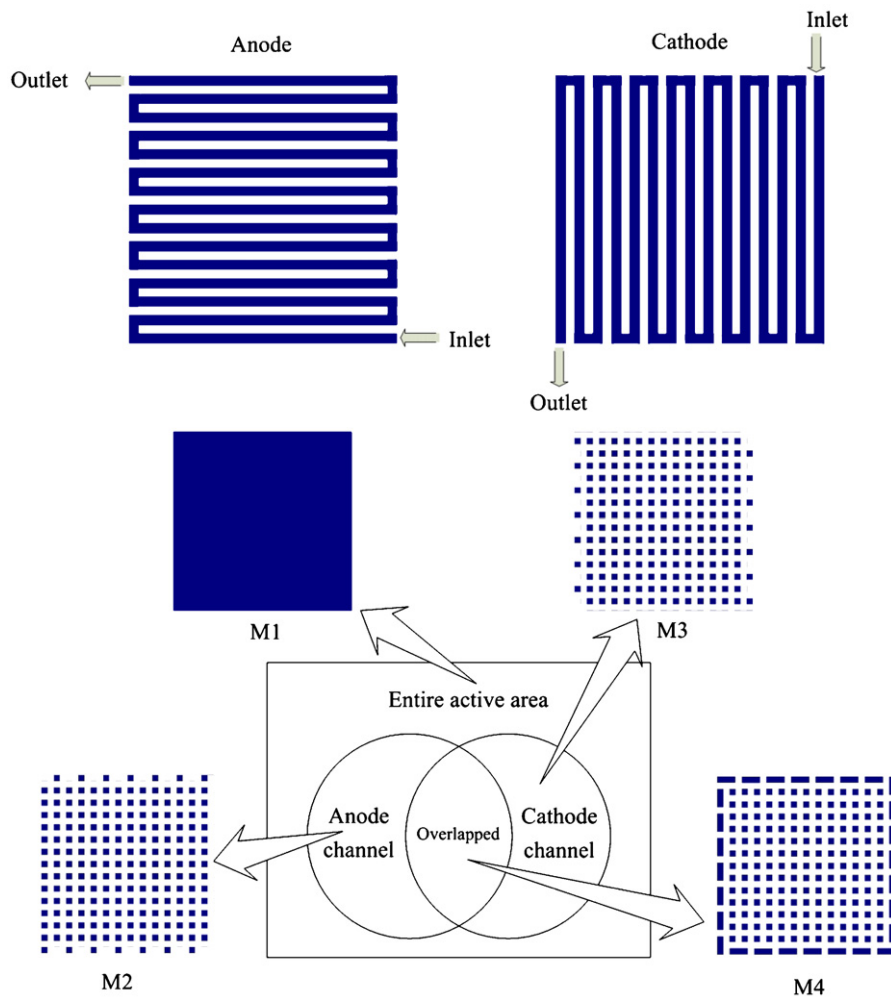


Fig. 2 – Flow channel layouts and masks used for post-processing of the neutron images.

that of oxygen for the cathode stream. The amount of water at the inlet of the cell is calculated based on the inlet pressure and temperature. For instance on the anode side,

$$Y_{H_2O,A_In} = \frac{RH_A P_{sat}(T)}{P_{A_In}}, \quad (4)$$

where Y_{H_2O,A_In} is the mole fraction of water vapor at the anode channel inlet, RH_A is the relative humidity, $P_{sat}(T)$ is the saturation pressure of the water vapor and P_{A_In} is the pressure at the inlet of the anode channel. Then, the flow rate of the water vapor is determined as:

$$\dot{N}_{H_2O,A_In} = \frac{Y_{H_2O,A_In} \dot{N}_{H_2,A_In}}{(1 - Y_{H_2O,A_In})}, \quad (5)$$

where \dot{N}_{H_2,A_In} is the molar flow of water vapor at the inlet of the anode.

The mass must be conserved at every node except at the reaction site. The rate of hydrogen consumption at the reaction site depends on the current density and it is calculated using Faraday's law:

$$\Delta \dot{N}_{R,H_2} = \frac{JA_{cell}}{2F}. \quad (6)$$

The mass balance in the anode side (the total consumption rate of reactant gas at the exit of anode reaction site) can be

written as follows:

$$\Delta \dot{N}_A = \Delta \dot{N}_{R,H_2} + (\dot{N}_{drag,H_2O} - \dot{N}_{back_diff,H_2O}), \quad (7)$$

where \dot{N}_{drag,H_2O} is the water transport from the anode to the cathode due to the electroosmotic drag effect and \dot{N}_{back_diff,H_2O} is the water transport by back diffusion from the cathode to the anode through the electrolyte membrane. In the cathode catalyst layer, oxygen is consumed and water a molecule is produced by the chemical reaction. The resultant mass balance in the cathode side (the consumption rate at the exit of the reaction site) is

$$\Delta \dot{N}_C = \Delta \dot{N}_{R,O_2} - \Delta \dot{N}_{R,H_2O} - (\dot{N}_{drag,H_2O} - \dot{N}_{back_diff,H_2O}). \quad (8)$$

The consumption rate of oxygen, $\Delta \dot{N}_{R,O_2}$, and the production rate of water, $\Delta \dot{N}_{R,H_2O}$, are given in terms of current density, J , and active area, A_{cell} :

$$\Delta \dot{N}_{R,O_2} = -\frac{JA_{cell}}{4F}, \quad (9)$$

$$\Delta \dot{N}_{R,H_2O} = \frac{JA_{cell}}{2F}. \quad (10)$$

The back diffusion and electroosmotic drag effect can be neglected, or do not have to be considered explicitly, in this mathematical model since the total amount of liquid water at

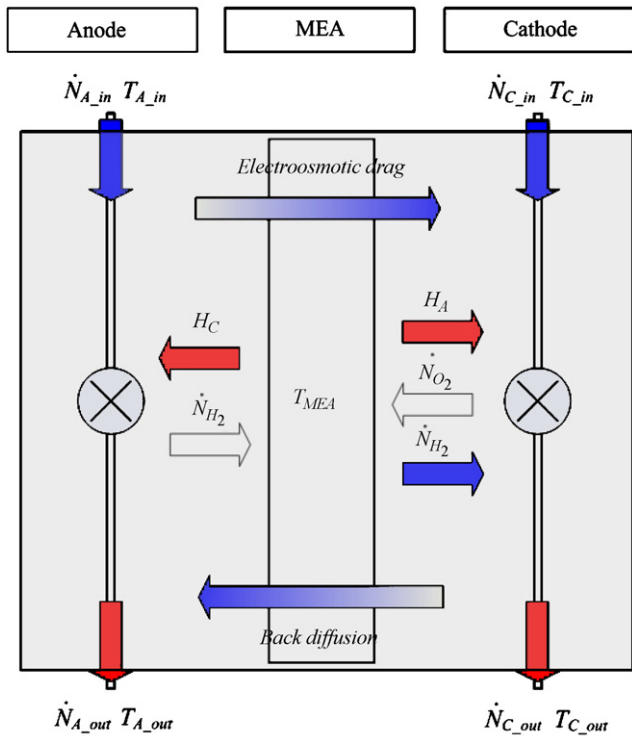


Fig. 3 – Schematic flow diagram of heat and mass transfer in a PEM fuel cell.

the exit of the anode and cathode together, which is the purpose of this analysis, is not affected by the results of these two phenomena. This is because for the present study the gas stream is fully saturated, and the cell is maintained isothermal and uniform temperature throughout the cell, since water vapor saturation is fully dependent on the temperature, which is fixed, the total amount of the liquid water at the cell exit will be the same, independent of the water transport between the anode and the cathode within the cell. Water condensation occurs as the amount of vapor water increases beyond its local saturation value. Hence, four species may exist at the cathode channel exit, including oxygen, liquid water, water vapor and nitrogen while three species may exist at the anode channel exit, including hydrogen, liquid water and water vapor. In reality, cathode gas may cross over to the anode side, however this crossover effect will not affect the results of the present analysis, hence it is not considered.

The pressure drop caused by frictional loss on the inside wall of flow channel is estimated based on Darcy–Weisbach equation [31]:

$$\Delta P = C_f \frac{L \rho V^2}{d_h} \quad (11)$$

where L is the length of the loop segment, D is the hydraulic diameter, ρ is the fluid average density, and V is the flow speed, and C_f is the friction coefficient determined from the following correlation [31]:

$$C_f = \begin{cases} C_{cr,l} C_1 / Re_{d_h} & (Re_{d_h} < 2 \times 10^3), \\ C_{cr,t} 0.316 / Re_{d_h}^{1/4} & (4 \times 10^3 < Re_{d_h} < 10^5), \end{cases} \quad (12)$$

where C_1 is a constant depending on the flow path geometry. However, the amount of pressure drop measured in the experiment is substantially lower than the value calculated from Eq. (11) due to the strong cross leakage flow in a PEM fuel cell [25,26]. $C_{cr,l}$ and $C_{cr,t}$ were introduced to account for this phenomenon so that the amount of pressure drop was modified to equal the measured pressure drop in the present experiment. The Reynolds number in Eq. (12) is defined based on the hydraulic diameter of each flow segment with μ representing the mixture viscosity:

$$Re_{d_h} = \frac{\rho V d_h}{\mu} \quad (13)$$

The value of C_f is linearly interpolated for the value of Re between 2000 and 4000. In the anode and cathode streams, the volumetric flow rate is obtained based on the ideal gas law as follows:

$$Q = \sum_k \frac{\dot{N}_k R T}{P_k} \quad (14)$$

where k is the species number, \dot{N}_k and P_k are the molar flow rate and partial pressure of the species k , respectively. Liquid volume was neglected in the calculation of volumetric flow rate. All properties of mixture gases are determined from the local composition and temperature [27]. It has been assumed that the temperature increment from the inlet to the exit of the flow channel is negligible. This assumption is justified by the following facts. First, the temperature gradient in the fuel cell cannot be significant since most materials of fuel cell elements such as graphite, copper and aluminum plates are good thermal conductors. Second, all temperatures including cell temperature and the inlet temperatures of fuel and oxidant are controlled equally by the heating and cooling system. To minimize the temperature gradient caused by a single rod type heater [21], the PEM fuel cell is heated from the wide area using a thin and long band type heater which wraps around the periphery of the cell assembly.

3. Results and discussion

3.1. Effect of load dynamics on the liquid water distribution

To satisfy the various demands of a power source for practical applications, a PEM fuel cell must ensure stable operation against load (current density) changes. Investigation on the dynamic performance response to a load variation would be useful for applying PEM fuel cells to practical applications, especially, transportation. Fig. 4 shows colorized neutron images for various current densities defined as Case I in Table 2. The current density was changed every 3 min with each image representing the integration of the last minute out of each 3 min duration. The characteristics of liquid water accumulation and distribution in the test PEM fuel cell can be summarized as described below.

Liquid water is not accumulated in the cathode flow channel since the flow speed is very high (up to 40 m/s) in the flow channel. Water clogging cannot occur in this situation. This was confirmed by the fact that no single

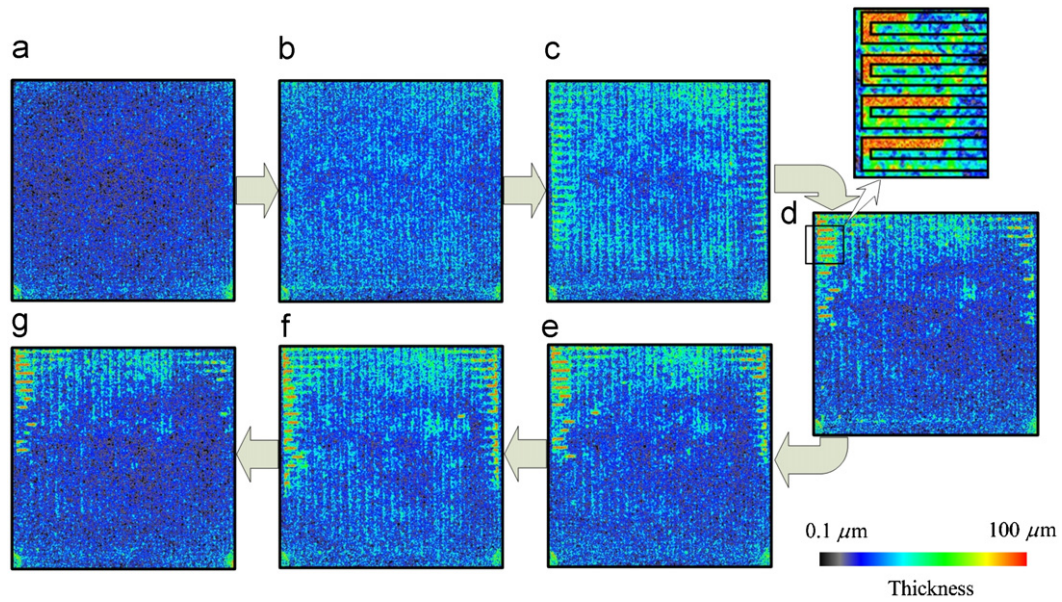


Fig. 4 – Colorized neutron images at different current densities for Case I, cell operating temperature of $T_c = 60^\circ\text{C}$, and 3 min duration for each load. Anode and cathode flow channel layouts are shown in Fig. 1. (a,g) 0.05 A/cm^2 , (b,f) 0.25 A/cm^2 , (c,e) 0.5 A/cm^2 and (d) 0.75 A/cm^2 .

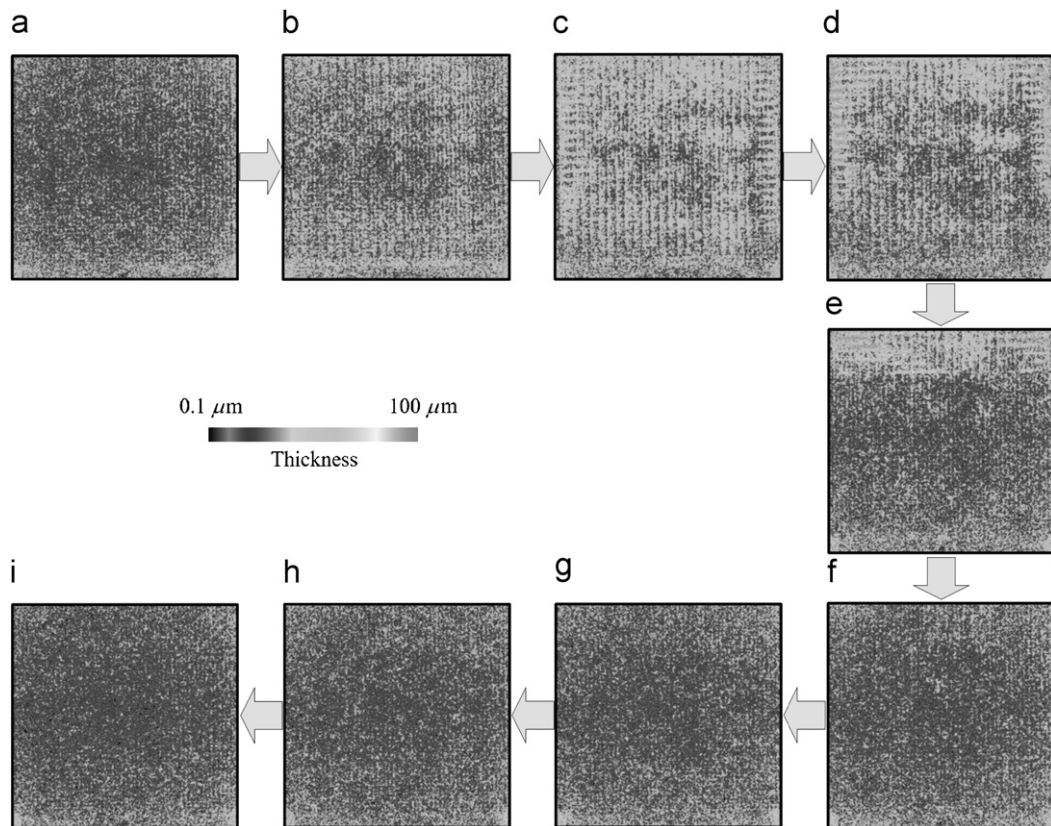


Fig. 5 – Colorized neutron images at the different current densities for Case II, cell operating temperature of $T_c = 60^\circ\text{C}$, and 3 min duration for each load. Anode and cathode flow channel layouts are shown in Fig. 1. (a,i) 0.05 A/cm^2 , (b,h) 0.25 A/cm^2 , (c,g) 0.5 A/cm^2 , (d,f) 0.75 A/cm^2 and (e) 1.0 A/cm^2 .

neutron image shows any noticeable water droplet in the flow channel area. As shown in a magnified view in Fig. 4, liquid water tends to accumulate in the GDL above the flow channel

area, in contrast to most of the previous observations, e.g., [21,22], which reported that liquid water was accumulated in the GDL segment adjacent to the channel land area.

This phenomenon can be attributed to the effect of the strong cross leakage flow in the test PEM fuel cell with a thin and long serpentine flow channel [24,25], i.e., the liquid water accumulated in the GDL above the channel land area is removed effectively by the cross leakage flow. However, the liquid water is not removed in the GDL above the flow channel since the cross leakage flow is very weak there.

Figs. 4(a)–(c) indicate that the amount of liquid water in the cell structure increases with increasing current density. The liquid water seems uniformly distributed in the cell, both anode and cathode side. At the peak current density of 0.75 A/cm^2 liquid water is not observed near the anode inlet, and increasing water content is observed towards the anode channel exit. The liquid water on the cathode seems to be more uniformly distributed. However, when the cell current density is decreased from 0.75 to 0.05 A/cm^2 , a completely different distribution of liquid water is observed, by comparing Figs. 4(e)–(g) with Figs. 4(a)–(c), even under the nominally identical conditions of the same current density and flow conditions. About half the anode side near the channel inlet is free of liquid water; liquid water is also observed around the channel turn regions near the middle of the anode side, and then increases significantly towards the anode channel exit. In contrast, the cathode side actually has less liquid water

and seems to be more uniformly distributed, without a clear accumulation of liquid water in the channel turn regions. This seems to contradict intuition since water is produced in the cathode side and electroosmotic drag also transports water to the cathode side. This seems to suggest that the cathode gas stream is very effective in removing water in the cathode. The apparently different distribution of liquid water with the seemingly identical operating conditions shown in Figs. 4(a)–(c) and (e)–(g) is responsible for the unreliable and unrepeatable PEM fuel cell performance observed in early studies [28].

Fig. 5 shows the neutron images for the same dynamic load variations as for Fig. 4, except that the maximum current density is increased from 0.75 A/cm^2 for Fig. 4 to 1.0 A/cm^2 for Fig. 5. The liquid water distribution shown in Figs. 5(a)–(d) is fairly similar to that in Figs. 4(a)–(d) for the same current density with uniform distribution and increasing thickness as the current density is increased from 0.05 to 0.75 A/cm^2 . However, for the peak current density of 1.0 A/cm^2 liquid water is only observed to exist in the last few anode channels near the anode channel exit without liquid water accumulation in the channel turn areas. Little liquid water is observed for the cathode and the significant portion of the anode away from the anode channel exit. The entire cell seems to be free

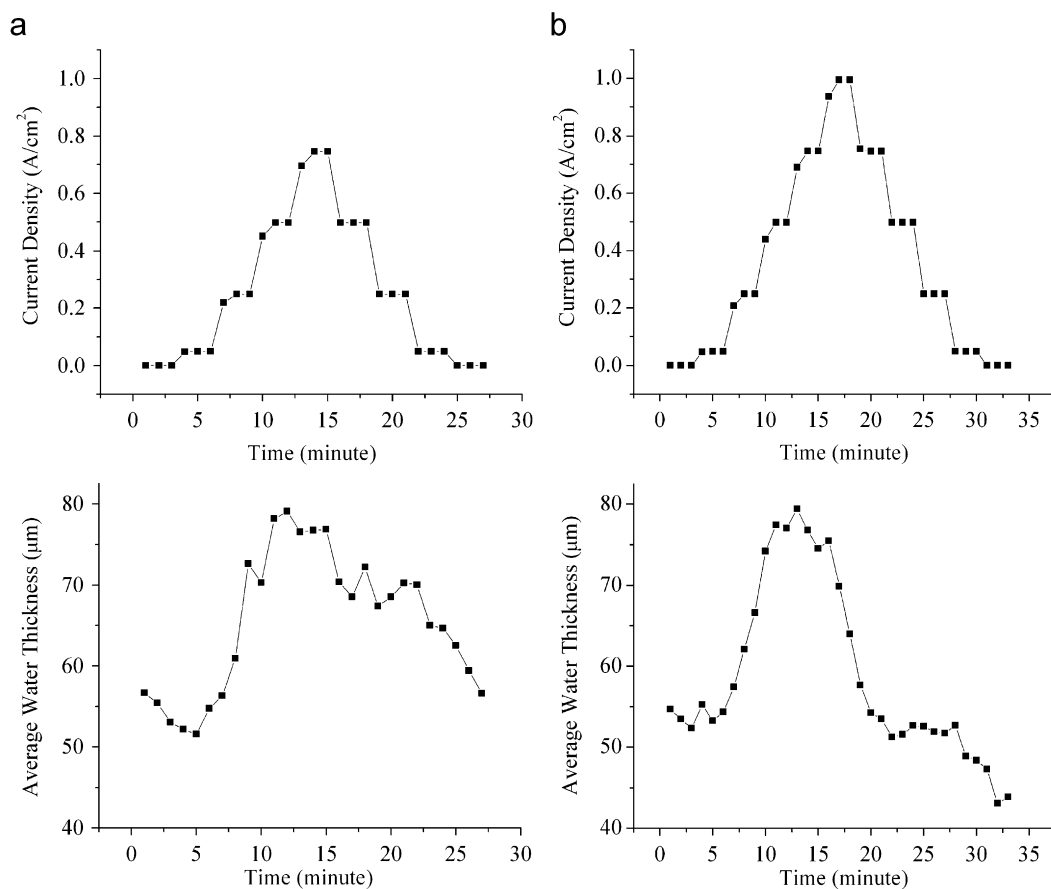


Fig. 6 – Equivalent average liquid water thickness in the entire test cell corresponding to the test conditions of Fig. 4 (a) and Fig. 5 (b); the uncertainty of each average water thickness (the standard deviation of mean average water thickness) ranges ± 1.42 – $2.16 \mu\text{m}$ with 95% probability.

of liquid water presence when the cell current density is reduced from the peak value of 1.0 to the minimum value of 0.05 A/cm². Clearly, the amount and distribution of the liquid water in the cell differs significantly in proportion to the current density. The hysteresis phenomenon in the quantity and distribution of liquid water in the cell clearly leads to the hysteresis in the cell performance.

The results shown in Figs. 4 and 5 are measured at the cell operating temperature of 60 °C. At the higher cell operating temperature of 80 °C, very little liquid water is detected by the neutron imaging technique, suggesting that liquid water flooding may not be a problem at that temperature, although the possibility of cell dehydration occurs then.

3.2. Performance hysteresis: the effect of liquid water accumulation and distribution

Figs. 6(a) and (b) show the dynamic response of the current density and liquid water in the cell for the conditions identical to those of Figs. 4 and 5, respectively. The current density shown is the measured response of the test cell when the current density is set for 3 min for each load condition. It is seen for both cases shown in Fig. 6 that when the load is increased, the current density responds to the load change very quickly for the low values of the current densities (0.0 and 0.05 A/cm²), then the response is slowed for the higher current densities of 0.25, 0.50, 0.75 and 1.0 A/cm². However, the response is again very fast when the load is reduced. These different dynamic responses are due to the formation and accumulation of liquid water in the cell as shown in Figs. 4 and 5. The response slows as current density increases, due to more liquid water formation and presence in the cell structure as shown in Figs. 4(a)–(d) and 5(a)–(e). The amount of liquid water decreases with decreasing load as shown in Figs. 4(e)–(g), with virtually no liquid present in Figs. 5(f)–(i). As a result, the performance response is fast. These observations are consistent with the numerical simulation of the dynamic responses for PEM fuel cells [29].

Fig. 6 also shows the equivalent average thickness of liquid water in the test cell (obtained from the neutron images and presented below the current density response for the two cases investigated). The amount of liquid water increases with increasing current density and reaches the maximum when the current density is increased to 0.5 A/cm² for both cases. Then the liquid water content is reduced even when the current density is further increased to the peak value and then decreased. As also indicated in the previous section, the amount of liquid water is much less for Case II (Fig. 5) than that for Case I (Fig. 4) after reaching the peak value of the liquid water accumulation. Different amounts of liquid water in the cell explains the difference in the performance hysteresis with load changes, as shown in Fig. 7. Case I highlights (corresponding to the test conditions for Fig. 4) that the cell performance is slightly better for the decreasing sweep of current density than the sweep of increasing current density. This result agrees with the observations made by Zhang et al. [21], who attributed it to a reduced surface coverage of the cathode with OH adsorbates [15] and a reduced ohmic resistance. In contrast to Case I, a lower performance is observed for Case II, corresponding to the

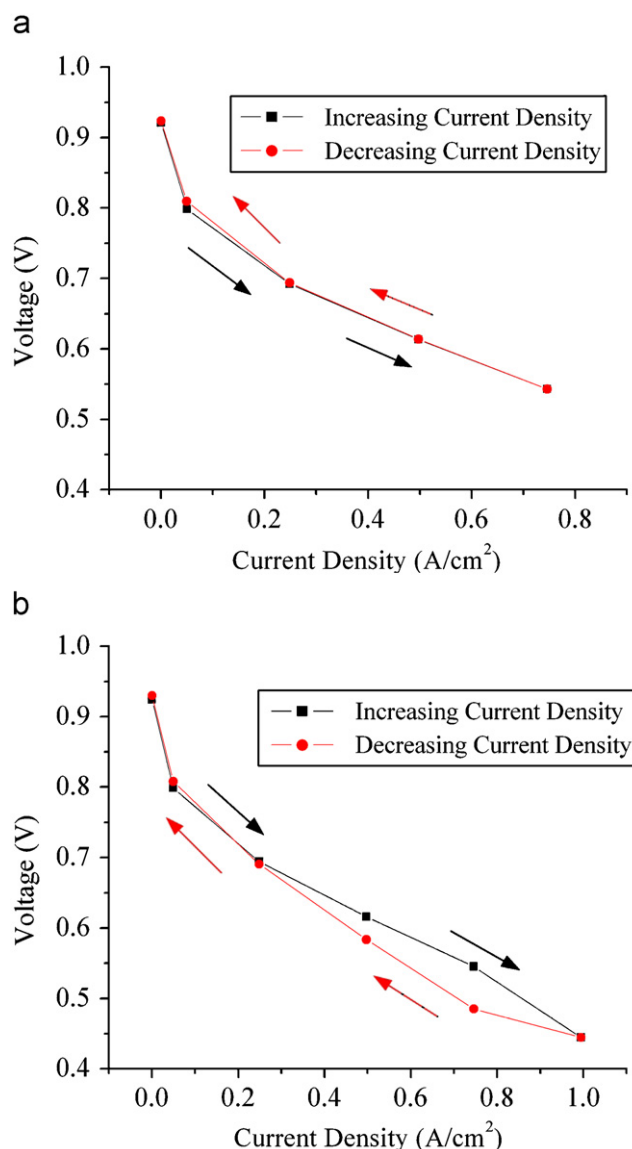


Fig. 7 – Dynamic cell performance corresponding to the test conditions of Fig. 4 (a) and Fig. 5 (b).

conditions for Fig. 5, for the sweep of decreasing current density. The voltage recovers to that of the increasing current density sweep when the current density is decreased to 0.25 A/cm². Finally, it should be pointed out that the characteristics of liquid water formation and accumulation as well as the associated performance hysteresis are almost identical to the results shown in Figs. 4–7 when the current density was changed every 5 min; hence, they are not shown here.

3.3. Mathematical modeling of liquid water production and the effect of temperature

Experimental investigation concerning the effect of cell temperature on the formation of liquid water in a PEM fuel cell can be found in Liu et al. [9] and Hickner et al. [23]. Hickner et al. [23] showed that the rate of liquid water production in a PEM fuel cell can become negative at high

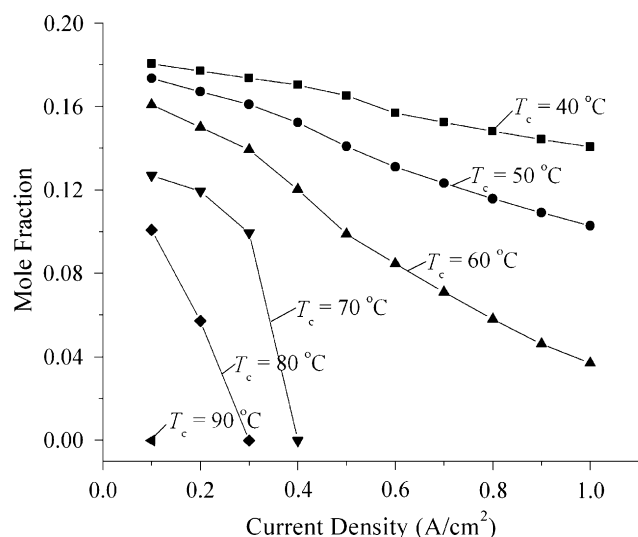


Fig. 8 – Model predictions for the mole fraction of liquid water at the exit of the test cell for various cell operating temperatures.

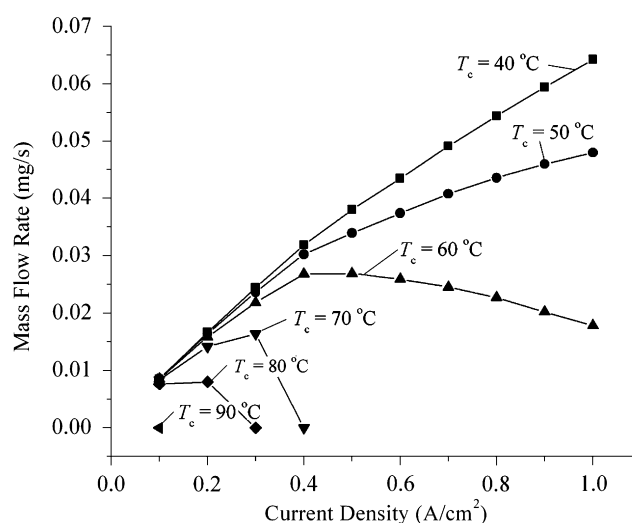


Fig. 9 – Model predictions for the mass flow rate of liquid water at the exit of the test cell for various cell operating temperatures.

temperatures (above 80 °C) due to evaporation and lower partial pressure of water. Liu et al. [9] visualized the inside of the flow channels and showed that the amount of liquid water formation is substantially reduced at higher temperatures (>80 °C) due to evaporation. Since the liquid water accumulation is critical on the cell performance at high current densities, predicting the amount of liquid water formation in a PEM fuel cell would be highly beneficial for the practical design and operation of the system. This effect becomes increasingly important in transportation applications where dynamic loading is common.

Fig. 8 shows the total mole fraction of the liquid water at the exit of the anode and cathode flow channels, determined from the present model analysis. Here the mole fraction of liquid water is defined as the molar flow rate of liquid water from both the anode and cathode channel exits divided by the total molar flow rate of all the species at the channel exits. It is seen that the molar fraction of the liquid water decreases consistently as the current density increases for all temperatures analyzed. This phenomenon is mainly caused by two reasons: first, the saturation pressure of water depends on the temperature only, and is independent of the reactant flow rate, hence it is independent of the current density since the stoichiometry for both the anode and cathode stream is fixed in the present study, as shown in Table 2. Second, as the current density increases, the reactant flow rate increases proportionally for the fixed stoichiometries, resulting in a larger pressure drop in the cell, because the frictional and minor pressure loss mechanisms are predominant, relative to the effect of reactant gas consumption in the cell, for the present channel design of small but long serpentine channels [26]. A larger pressure drop in the cell for the reactant gas streams results in (i) a relatively smaller amount of water vapor at the inlet of the flow channels because of a higher total pressure at the channel inlet (since in the present study the cell pressure is set at the channel exit) and (ii) more water removal in vapor

form [1]. As a result, the amount of liquid water remaining at the channel exit is reduced as the reactant gas flow rate and current density increases. Fig. 8 also shows that the amount of liquid water at the channel exits decreases as the cell operating temperature increases due to the higher vapor capacity of the gas stream in vaporizing liquid water [1]. For the operating temperature of 70 °C, the mole fraction of liquid water becomes zero at the current density of about 0.4 A/cm². When the operating temperature exceeds 90 °C the mole fraction of liquid water drops to zero for the entire current density range of interest.

Fig. 9 shows the total mass flow rate of liquid water at the channel exits calculated from the mole fraction given in Fig. 8. Similar to the mole fraction, the liquid mass flow rate decreases as the cell temperature is increased due to a higher water removal capacity of the gas stream in the form of water vapor. Unlike the mole fraction shown in Fig. 8, the amount of liquid water flow increases consistently as the current density is increased for the cell temperature below ~60 °C. When the cell operating temperature is at or above 60 °C, the liquid water mass flow rate increases with current density until reaching a maximum value, beyond which it starts to decrease for further increase in the current density. This occurs since at low current densities, the reactant flow rate is low and thus water production as a result of cell reaction dominates. As the current density increases, reactant gas flow increases, and the pressure drop becomes substantial. Thus, more water is removed from the cell in the form of vapor resulting in a lower liquid water mass flow rate at the channel exits. Although the present model calculates the rate of net liquid water production in a steady-state condition the result could be useful to predict the trend of liquid water accumulation especially when the cell has a quick response against the load change. It is noticed that the value of current density at the maximum liquid water mass flow rate in Fig. 9 ($T_c = 60$ °C), about 0.5 A/cm², coincides with the peak water accumulation in Fig. 6.

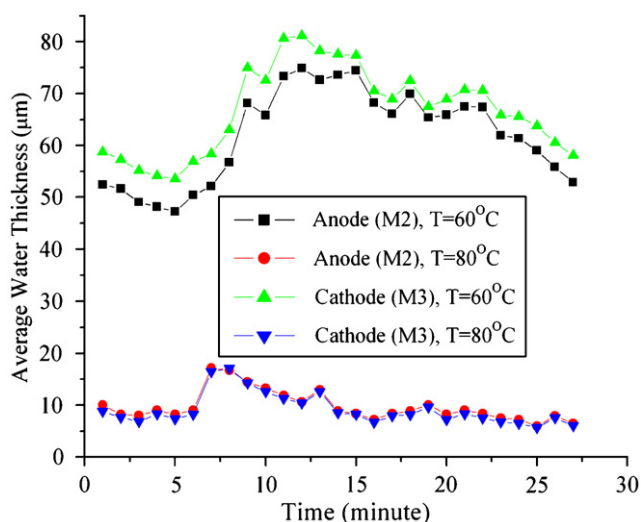


Fig. 10 – Equivalent average liquid water thickness in the test cell as measured from the neutron imaging technique for different cell operating temperatures under the dynamic loading condition of Case I. The current density variation with time is given in Fig. 6.

Fig. 10 shows the total amount of liquid water in the test cell (determined by the neutron images), for two different operating temperatures (60 and 80 °C) under the same load variations (Case I). The amount of liquid water in the cell is much less when the temperature is higher (80 °C). Note that the peak water accumulation occurs at the current density of 0.25 A/cm², which agrees again with the modeling results shown in Fig. 9 for the temperature of 80 °C. At this operating temperature, the cell could not sustain its voltage at 1 A/cm² at the operating temperature of 80 °C; however, such temporal and short-duration dehydration did not seem to result in any permanent damage on the membrane, because the same performance was measured in repeated tests under other operating conditions. On the other hand, significantly more liquid water is present in the cell at the cell temperature of 60 °C, as also implied by the model results shown in Fig. 9, and the peak value of the liquid water accumulation in the cell, about 0.5 A/cm² in Fig. 10, also agrees with the model results shown in Fig. 9.

4. Conclusions

In this study, the amount and distribution of liquid water in an operating PEM fuel cell with a single serpentine flow channel for the anode and cathode side has been investigated under dynamic loading using neutron imaging technique. It is observed that liquid water accumulation in the cell generally reduces or slows down the dynamic response of the fuel cell to changing load conditions. In addition, performance hysteresis is also observed due to the different amount of liquid water content in the cell at the nominally identical operating conditions. The amount of liquid water accumulation in the cell is dependent on the cell operating temperature, the pressure drop in the flow channel and the current density. It is shown that the cell performance is strongly

affected by the presence and accumulation of liquid water, especially at high current densities. The rate of liquid water production is also mathematically modeled to analyze the effect of the cell operating temperature and pressure drop on the liquid water formation in a cell. The model predicts successfully the trend of liquid water accumulation in an operating PEM fuel cell. Finally, the history of liquid water accumulation is also analyzed.

Acknowledgments

This work was financially supported by AUTO21, the Network of Centers of Excellence, Canada, the DaimlerChrysler Corporation, and the U.S. Department of Commerce, the NIST Ionizing Radiation Division, the Director's office of NIST, the NIST Center for Neutron Research, and the Department of Energy through interagency agreement no. DE-AI01-01EE50660.

REFERENCES

- [1] Li X. Principles of fuel cells. New York: Taylor & Francis; 2006.
- [2] Tuber K, Pczar D, Hebling C. Visualization of water buildup in the cathode of a transparent PEM fuel cell. *J Power Sources* 2003;124:403–14.
- [3] Nguyen TV. A gas distributor design for proton-exchange-membrane fuel cells. *J Electrochem Soc* 2002;143(5):L103–5.
- [4] Mench MM, Dong Q, Wang CY. In situ water distribution measurements in a polymer electrolyte fuel cell. *J Power Sources* 2003;124:90–8.
- [5] Stumper J, Lhr M, Hamada S. Diagnostic tools for liquid water in PEM fuel cells. *J Power Sources* 2005;143:150–7.
- [6] Hakenjos A, Muentner H, Wittstadt U, Hebling C. A PEM fuel cell for combined measurement of current and temperature distribution, and flow field flooding. *J Power Sources* 2004;131:213–6.
- [7] Yang X, Zhang F, Lubawy L, Wang CY. Visualization of liquid water transport in a PEFC. *Electrochem Solid-State Lett* 2004;7(11):A408–11.
- [8] Sugiura K, Nakata M, Yodo T, Nishiguchi Y, Yamauchi M, Itoh Y. Evaluation of a cathode gas channel with a water absorption layer/waste channel in a PEFC by using visualization technique. *J Power Sources* 2005;145:526–33.
- [9] Liu X, Guo H, Ma C. Water flooding and two-phase flow in cathode channels of proton exchange membrane fuel cells. *J Power Sources* 2006;156:267–80.
- [10] Nam J, Kaviany M. Effective diffusivity and water-saturation distribution in single- and two-layer PEMFC diffusion medium. *Int J Heat and Mass Transfer* 2003;46:4595–611.
- [11] Lim C, Wang CY. Effects of hydrophobic polymer content in GDL on power performance of a PEM fuel cell. *Electrochim Acta* 2004;49:4149–56.
- [12] Feindel K, LaRocque L-A, Starke D, Bergens S, Wasylishen R. In situ observations of water production and distribution in an operating H₂/O₂ PEM fuel cell assembly using 1H NMR microscopy. *J Am Chem Soc* 2004;126:11436–7.
- [13] Tsushima S, Teranishi K, Nishida K, Hirai S. Water content distribution in a polymer electrolyte membrane for advanced fuel cell system with liquid water supply. *Magn Reson Imaging* 2005;23:255–8.
- [14] Mosdale R, Gebel G, Pineri M. Water profile determination in a running proton exchange membrane fuel cell using small-angle neutron scattering. *J Membr Sci* 1996;118:269–77.

- [15] Bellows RJ, Lin MY, Arif M, Thompson AK, Jacobson D. Neutron imaging for in situ measurement of water transport gradients within Nafion in polymer electrolyte fuel cells. *J Electrochem Soc* 1999;146:1099–103.
- [16] Satija R, Jacobson DL, Arif M, Werner SA. In situ neutron imaging technique for evaluation of water management systems in operating PEM fuel cells. *J Power Sources* 2004;129:238–45.
- [17] Kramer D, Zhang J, Shimoi R, Lehmann E, Wokaun A, Shinohara K, et al. In situ diagnostic of two-phase flow phenomena in polymer electrolyte fuel cells by neutron imaging part A. Experimental, data treatment, and quantification. *Electrochim Acta* 2005;50:2603–14.
- [18] Kramer D, Lehmann E, Frei G, Vontobel P, Wokaun A, Scherer G. An on-line study of fuel cell behavior by thermal neutrons. *Nucl Instrum Methods Phys Res A* 2005;542:52–60.
- [19] Pekula N, Heller K, Chuang P, Turhan A, Mench MM, Brenizer J, et al. Study of water distribution and transport in a polymer electrolyte fuel cell using neutron imaging. *Nucl Instrum Methods Phys Res A* 2005;542:134–41.
- [20] Turhan A, Heller K, Brenizer JS, Mench MM. Quantification of liquid water accumulation and distribution in a polymer electrolyte fuel cell using neutron imaging. *J Power Sources*, in press.
- [21] Zhang J, Kramer D, Shimoi R, Ono Y, Lehmann E, Wokaun A, et al. In situ diagnostic of two-phase flow phenomena in polymer electrolyte fuel cells by neutron imaging part B. Material variations. *Electrochim Acta* 2006;51:2715–27.
- [22] Chuang PA, Turhan A, Heller AK, Brenizer JS, Trabold TA, Mench MM. Real-time imaging of liquid water in an operating proton exchange membrane fuel cell. In: Proceedings of FUELCELL2005 third international conference on fuel cell science, engineering and technology, May 23–25, 2005, Ypsilanti, Michigan, USA.
- [23] Hickner MA, Siegel NP, Chen KS, Mcbrayer DN, Hussey DS, Jacobson DL, et al. Real-time imaging of liquid water in an operating proton exchange membrane fuel cell. *J Electrochem Soc* 2003;153(5):A902–8.
- [24] Kanezaki K, Li X, Baschuk JJ. Cross-leakage flow between adjacent flow channels in PEM fuel cells. *J Power Sources* 2006;162:415–25.
- [25] Park J, Li X. An experimental and numerical investigation on the cross flow through gas diffusion layer in a PEM fuel cell with a serpentine flow channel. *J Power Sources* 2007;163:853–63.
- [26] Li X, Sabir I, Park J. A flow channel design procedure for PEM fuel cells with effective water removal. *J Power Sources* 2007;163:933–42.
- [27] Baschuk JJ, Li X. Mathematical model of a PEM fuel cell incorporating CO poisoning and O₂ (air) bleeding. *Int J Global Energy Issues* 2003;20(3):245–76.
- [28] Mughal A, Li X. Experimental diagnostics of PEM fuel cells. *Int J Environ Stud* 2006;63:377–89.
- [29] Wu H, Li X, Berg P. Numerical analysis of dynamic processes in fully humidified PEM fuel cells. *Intl J Hydrogen Energy* 2007;32:2022–31.
- [31] White FM. Fluid mechanics. 3rd ed. New York: McGraw-Hill; 1994.
- [32] Jiao K, Zhou B, Quan P. Liquid water transport in parallel serpentine channels with manifolds on cathode side of a PEM fuel cell stack. *J Power Sources* 2006;154:124–37.
- [33] Shimpalee S, Greenway S, Spuckler D, Van Zee JW. Predicting water and current distributions in a commercial-size PEMFC. *J Power Sources* 2004;135:79–87.
- [34] Wang ZH, Wang CY, Chen KS. Two-phase flow and transport in the air cathode of proton exchange membrane fuel cells. *J Power Sources* 2001;94:40–50.